Available online at www.sciencedirect.com
ScienceDirect
Journal of Power Sources 181 (2008) 17–23
JOURNAL OF POWER SOURCES
www.elsevier.com/locate/jpowsour

Properties of $BaCe_{1-x}Ti_xO_3$ materials for hydrogen electrochemical separators

P. Pasierb *, E. Drożdż-Cieśla, M. Rekas

AGH University of Science and Technology, Faculty of Materials Science and Ceramics, al. Mickiewicza 30, 30-059 Krakow, Poland

Received 30 September 2007; received in revised form 15 November 2007; accepted 30 November 2007
Available online 23 December 2007

Abstract

In this work the structural, microstructural and electrical properties of $BaCe_{1-x}Ti_xO_3$ materials were investigated. The series of materials with different titanium concentrations x (0–0.3) were prepared by solid-state reaction method. The structural studies by X-ray diffraction have shown that undoped material crystallizes in orthorhombic phase, while the increasing concentration of Ti dopant up to $x = 0.2$ leads to the ordering of the structure to phases with higher symmetries (tetragonal and even cubic). The estimated solubility limit was found to be not higher than 20 at.% of Ti. Microstructure observations by scanning electron microscopy and linear contraction determination have shown the strong influence of Ti dopant on microstructure and an improvement of sinterability. The DC four-probe electrical conductivity measurements accompanied by the potentiometric EMF measurements of solid-state electrochemical cells in controlled gas atmospheres (containing H_2, O_2 and H_2O) and temperatures (500–800 °C) allowed determination of the total and partial electrical conductivities of selected materials. It was found that the introduction of Ti dopant leads to a decrease in total electrical conductivity by ca. one order of magnitude compared to the undoped material, almost independently of Ti concentration. Also, the modification of transport properties after doping with titanium was determined.

Keywords: Protonic conductors; Barium cerate; Barium titanate; Solid solution; Hydrogen separation; Solid-state membranes

1. Introduction

Replacing traditional carbon-based fossil fuels by hydrogen is a very urgent need in 21st century. The approaching hydrogen era presents new challenges concerning production of clean hydrogen. Clean hydrogen can be produced using either electrolytic or photoelectrolytic splitting of water. However, electrolysis of water requires large amounts of electrical energy, which has a negative impact on environment [1,2]. On the other hand, the photoelectrolysis method suffers from very low efficiency [3,4]. It is well established that the main sources of hydrogen are based on gasification of coal or biomass, reforming or partial oxidation of hydrocarbons and hydrogen recovered from various by-products in chemical industry. Unfortunately, these methods provide hydrogen-containing contaminations, mainly carbon dioxide. Also, carbon monoxide, water vapor, hydrocarbons and gaseous compounds of sulphur can be present. Considering the fact that in addition to hydrogen, these methods generate large quantities of carbon dioxide, CO_2, i.e. the gas causing greenhouse effect, the problem to reduce CO_2 emission arises. It is possible to solve this problem by establishing the technology of hydrogen purification in which CO_2 is obtained in the concentrated form. Such CO_2 can be transported and stored in either geological formations or in oceans as carbonates, or may be used as a raw material in some industrial processes [5,6]. So, the development of an effective method of separation of hydrogen from CO_2 and other contaminant gases is an important challenge.

Electrochemical separation using hydrogen permeable membranes with the optimized properties seems to be the promising method for production of pure hydrogen in the future. This method requires neither sophisticated equipment nor use of any chemicals and pose no problems associated with utilization of by-product. The method is based on ionic transport

* Corresponding author. Tel.: +48 12 617 25 33; fax: +48 12 617 24 93.
E-mail address: ppasierb@agh.edu.pl (P. Pasierb).

0378-7753/$ – see front matter © 2007 Elsevier B.V. All rights reserved.
doi:10.1016/j.jpowsour.2007.11.114

of hydrogen in the proton form through the membrane. The material used as membrane separator should exhibit mixed protonic–electronic conductivity. On the other hand, if the membrane material exhibits purely protonic conductivity, then the hydrogen transport through the membrane must be enforced by external potential difference applied at both sides of the membrane.

The most promising membrane materials seem to be high-temperature proton-conducting substances based on strontium or barium cerates [7].

Unfortunately, the membrane separators have not found wider practical applications so far, due to the lack of suitable membrane materials with high rates of separation process and high stability against CO_2. The separation efficiency is correlated with the rate of charge transport (both electron holes and protons). Generally, this rate depends on the rate of gas/surface processes, transference numbers and resistivity of the electrolyte across the membrane. The second problem requires an improvement of the membrane stability, mainly in the presence of CO_2. One the most promising ways to achieve it is to choose a suitable chemical composition by doping cerate-based material with foreign ions [8–10].

This paper deals for the first time with the modification of structural, microstructural and electrical properties of barium cerate by doping it with titanium.

2. Materials preparation

Powders of $BaCe_{1-x}Ti_xO_3$ ($x = 0.0$, 0.05, 0.07, 0.10, 0.15, 0.20 and 0.30) were prepared by solid-state reaction method. Barium carbonate $BaCO_3$ (99.9%), cerium (IV) oxide CeO_2 (99.9%) and TiO_2 nanopowder (99.7%), all reagents as supplied by Aldrich Chemical Company, Inc., were used as starting materials. After mixing the appropriate amounts of starting powders, the materials were calcinated at 1200 °C for 24 h. The reaction of formation of barium cerium–titanium oxide can be written as follows:

$$BaCO_3 + (1-x)CeO_2 + xTiO_2 \Leftrightarrow BaCe_{(1-x)}Ti_xO_3 + CO_2 \quad (1)$$

The obtained materials were crushed in agate mortar, milled in the absolute alcohol suspension using a rotation–vibration mill and ZrO_2 grinding media, then formed in pellet die (Ø = 25 mm) at 25 MPa, isostatically pressed at 250 MPa and sintered at 1500 °C for 24 h in air atmosphere. Obtained sintered bodies were cut to the required size and shape.

Prior to electrical measurements, porous Pt electrodes were applied at both sides of every pellet (Demetron Pt paste fired at 850 °C (5 min). Additionally, the pellets of solid electrolytes designated for determination of transference numbers, after the application of Pt porous electrodes, were attached to alumina tubes (OD = 8 mm, ID = 5 mm) using the Ceramabond 569 ceramic adhesive. All obtained pellets of solid electrolytes were stored in dessicator before being used in further tests and experiments.

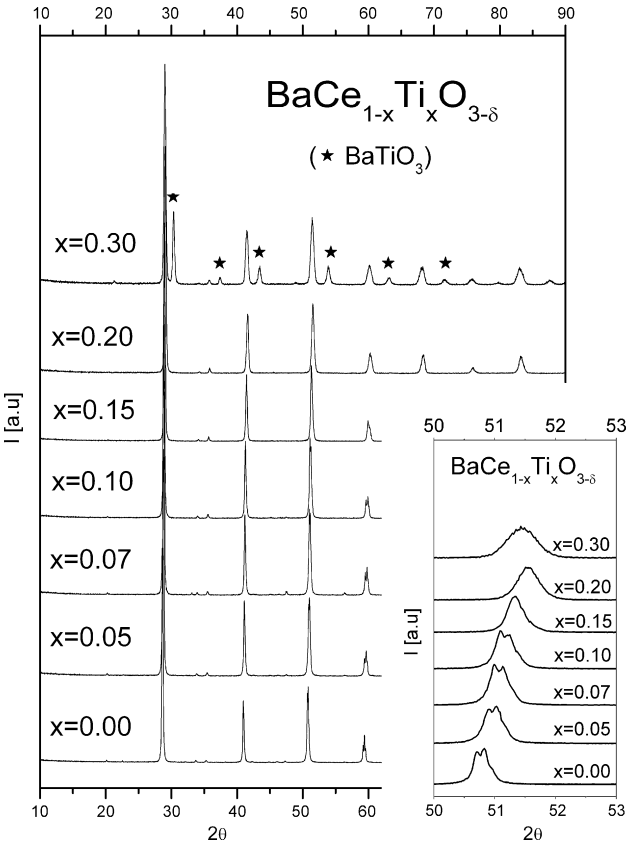

Fig. 1. XRD patterns of $BaCe_{1-x}Ti_xO_3$ sintered bodies ($T = 1500$ °C, 24 h).

3. Results and discussion

3.1. XRD data

XRD measurements were done using CuK_α radiation (Philips X'Pert) within the 2θ range 10–90° with the scan rate of 0.008° s^{-1}. Fig. 1 shows the XRD measurements of $BaCe_{1-x}Ti_xO_3$ pellets after sintering at 1500 °C for 24 h, as a function of Ti concentration (x). The magnification of 50°–53° 2θ range is shown in inset. Based on XRD results, undoped sample ($x = 0$) crystallized in orthorhombic Pmcn structure [11]. In the case of $BaCe_{1-x}Ti_xO_3$ samples with $0 \le x \le 0.20$, the incorporation of titanium into the lattice lead to a gradual ordering of the structure, probably according to the scheme: orthorhombic → tetragonal → cubic, which is observed in the inset as a disappearance of the reflex splitting with the increase of Ti concentration. Moreover, the shift of reflex maxima towards higher values of 2θ with the increase of Ti is observed, caused by the decrease of lattice constants. Further, more precise measurements are necessary in order to unequivocally determine the structure type and exact values of lattice constants.

The $BaCe_{0.7}Ti_{0.3}O_3$ sample ($x = 0.30$) showed additional reflexes originating from the second phase, which is probably $BaTiO_3$ tetragonal phase doped with cerium.

3.2. Microstructure

The SEM observations were done using NOVA NANO SEM scanning electron microscope. Additionally, the linear con-

traction (%) during sintering was determined based on the measurements of the sample size before and after sintering. The microphotographs were done on freshly prepared fractures, sputtered by a thin layer of carbon. Fig. 2A, shows the linear contraction (%) after sintering as a function of Ti concentration. As can be seen, the introduction of titanium leads to the abrupt increase of linear contraction, suggesting the higher density of the samples doped with Ti comparing to undoped $BaCeO_3$. Fig. 2B shows the SEM microphotographs of fractured $BaCe_{1-x}Ti_xO_3$ pellets sintered at 1500 °C for 24 h, as a function of x. The SEM observations have shown that dense materials were obtained in the case of all compositions. Both results presented in Fig. 2 indicate that introduction of titanium dopant leads to a substantial improvement of sinterability of doped materials compared to the undoped one.

3.3. Electrical properties: partial conductivities

Partial conductivities were determined from the DC four-probe electrical conductivity measurements and potentiometric EMF measurements of solid cells.

The DC conductivity measurements were done in the temperature range of 780–1090 K at two gas atmospheres: rich in oxygen ($pO_2 = 2 \times 10^4$ Pa) and rich in hydrogen H_2 (7 vol.% H_2 in Ar). Both atmospheres had the same level of humidity (100% RH at $T = 25$ °C). The required gas composition was obtained by mixing the gases at a proper ratio, using the MKS gas flow controllers and passing them through a water bubbler. Prior to each measurement, each sample was equilibrated at least 4–5 h under steady conditions. Table 1 compares the determined total conductivities of two samples: $BaCeO_3$ and $BaCe_{0.95}Ti_{0.05}O_3$.

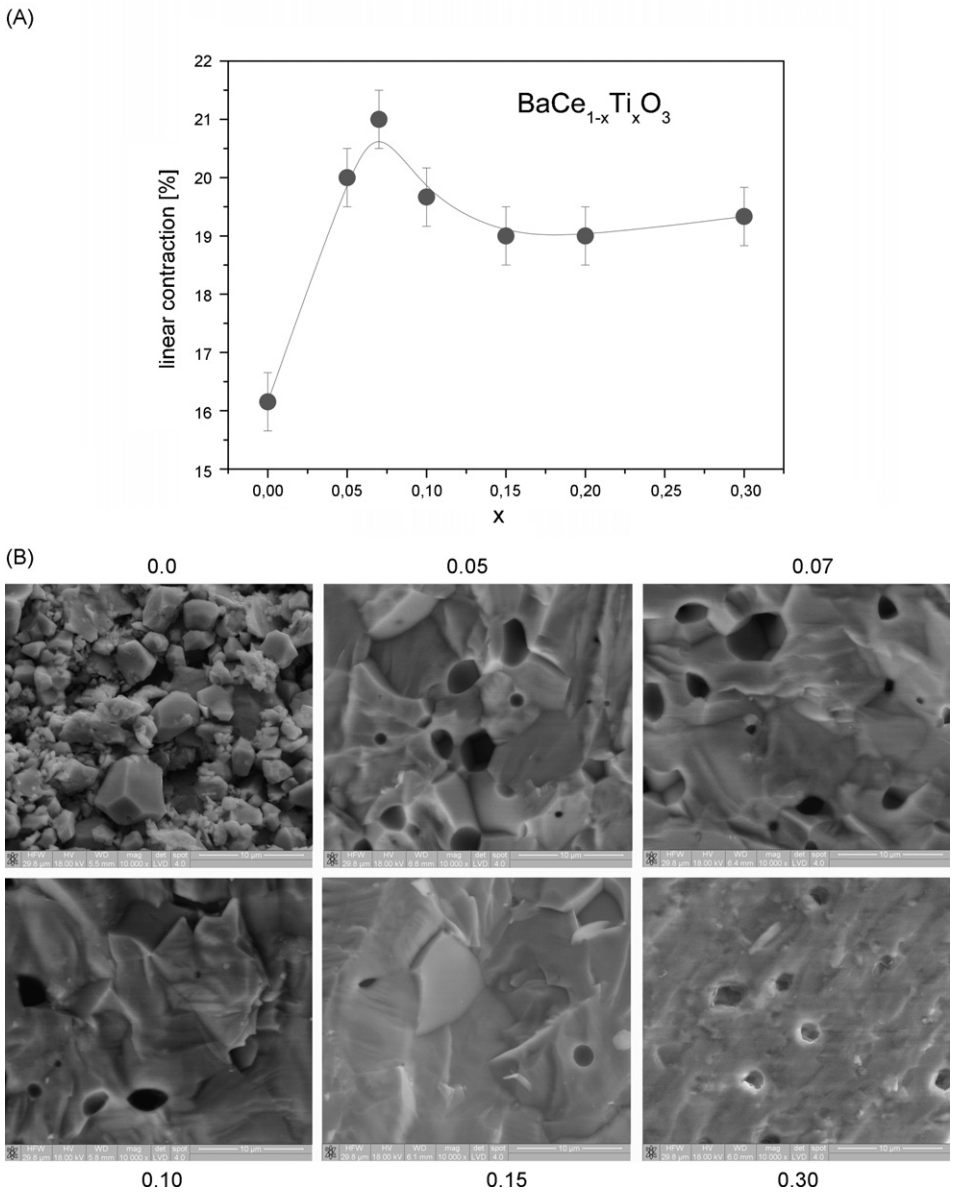

Fig. 2. (A) Linear contraction of pellets during sintering at 1500 °C for 24 h as a function of Ti concentration, (B) SEM microphotographs of fractured $BaCe_{1-x}Ti_xO_3$ pellets sintered at 1500 °C for 24 h.

Table 1
The comparison of total conductivities σ_{total} (Ω^{-1} cm^{-1}) of $BaCeO_3$ and $BaCe_{0.95}Ti_{0.05}O_3$ samples, determined using the DC four-probe measurements

T (°C)	$BaCeO_3$		$BaCe_{0.95}Ti_{0.05}O_3$	
	Oxygen rich atmosphere $p(O_2) = 21280$ Pa, $p(H_2O) = 3170$ Pa	Hydrogen rich atmosphere $p(H_2) = 7100$ Pa, $p(H_2O) = 3170$ Pa	Oxygen rich atmosphere $p(O_2) = 21280$ Pa, $p(H_2O) = 3170$ Pa	Hydrogen rich atmosphere $p(H_2) = 7100$ Pa, $p(H_2O) = 3170$ Pa
500	3.01×10^{-4}	3.74×10^{-4}	6.15×10^{-6}	2.70×10^{-5}
600	8.43×10^{-4}	8.58×10^{-4}	3.69×10^{-5}	4.94×10^{-5}
700	2.07×10^{-3}	1.39×10^{-3}	4.06×10^{-5}	2.85×10^{-4}
800	3.71×10^{-3}	1.85×10^{-3}	3.50×10^{-4}	5.54×10^{-4}

The $p(H_2O)$ corresponds to 100% RH at $T = 25$ °C

The total conductivities of the latter sample are representative for all doped samples ($x = 0.05$–0.20), as can be seen later in Fig. 7.

Potentiometric measurements of EMF versus temperature of solid cells manufactured from studied materials as solid electrolytes were performed in sample holder allowing the delivery of different gas atmospheres at both sides of the cells. The temperature and gas atmospheres applied were the same as in the case of DC four-probe conductivity measurements, as described above. The open cell voltage, E, of following cells was measured as a function of temperature:

$$\mathrm{Pt},\ p(\mathrm{X_2})^{(1)},\ p(\mathrm{H_2O})^{(1)} \mid \mathrm{BaCe_{1-x}Ti_xO_3} \mid p(\mathrm{X_2})^{(2)},\ p(\mathrm{H_2O})^{(2)},\ \mathrm{Pt} \quad (2)$$

where $p(X_2)^{(1)}$ and $p(X_2)^{(2)}$ describe the hydrogen or oxygen atmosphere with defined pressures at both sides of the cells, while $p(H_2O)^{(1)}$ and $p(H_2O)^{(2)}$ are the water vapor pressures. The pressures used are summarized in Table 2.

According to the considerations described in [12–14] the measurement of EMF of different electrochemical cells allows to determine the partial electrical conductivity realized by: oxygen ions (σ_O), protons (σ_H) and electrons (σ_{el}) or holes (σ_h):

$$E = \frac{RT}{4F}(t_O + t_H) \ln \frac{pO_2^{(2)}}{pO_2^{(1)}} - \frac{RT}{2F} t_H \ln \frac{pH_2O^{(2)}}{pH_2O^{(1)}} \quad (3)$$

$$E = \frac{RT}{2F}\left(t_O \ln \frac{pH_2O^{(2)}}{pH_2O^{(1)}} - (t_O + t_H) \ln \frac{pH_2^{(2)}}{pH_2^{(1)}} \right) \quad (4)$$

where $t_i = \sigma_i/\sigma_{total}$; i = O, H

Figs. 3–6 illustrate total (σ_{total}), ionic σ_{ion} ($\sigma_H + \sigma_O$) and partial (σ_H, σ_O, σ_{el}) electrical conductivities as a function of temperature of both $BaCeO_3$ and $BaCe_{0.95}Ti_{0.05}O_3$ samples, monitored at either hydrogen or air gas atmospheres. The $BaCeO_3$ in hydrogen rich atmosphere (Fig. 3) shows predominantly ionic conductivity, which is mainly realized by protons. Oxygen ion conductivity assumes very low values, close to zero.

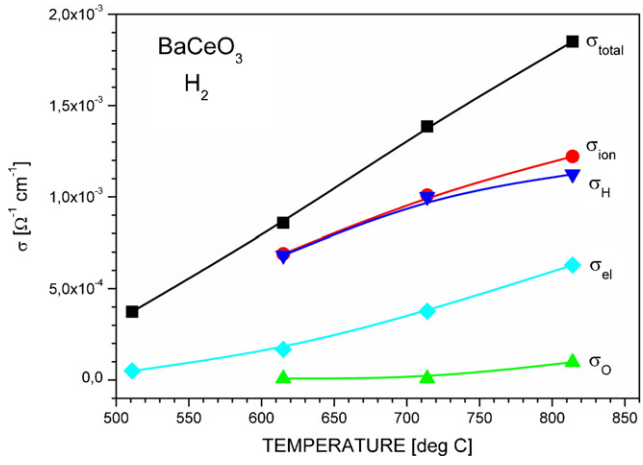

Fig. 3. Electrical conductivity versus temperature of $BaCeO_3$ in H_2 rich atmosphere (7 vol.% H_2 in Ar).

Table 2
The description of potentiometric cells used for the determination of partial electrical conductivity components

Cell	$p(O_2)^{(1)}$ or $p(H_2)^{(1)}$	$p(H_2O)^{(1)}$	$p(O_2)^{(2)}$ or $p(H_2)^{(2)}$	$p(H_2O)^{(2)}$
Oxygen containing atmospheres				
$p(O_2)$ gradient	21280	3170	2128	3170
	21280	3170	10640	3170
$p(O_2)$ and $p(H_2O)$ gradient	21280	635	2128	3170
$p(H_2O)$ gradient	21280	635	21280	3170
	21280	1585	21280	3170
Hydrogen containing atmospheres				
$p(H_2)$ gradient	7100	3170	710	3170
	7100	3170	3550	3170
$p(H_2)$ and $p(H_2O)$ gradient	7100	635	710	3170
$p(H_2O)$ gradient	7100	635	7100	3170
	7100	1585	7100	3170

Gas pressures in (Pa).

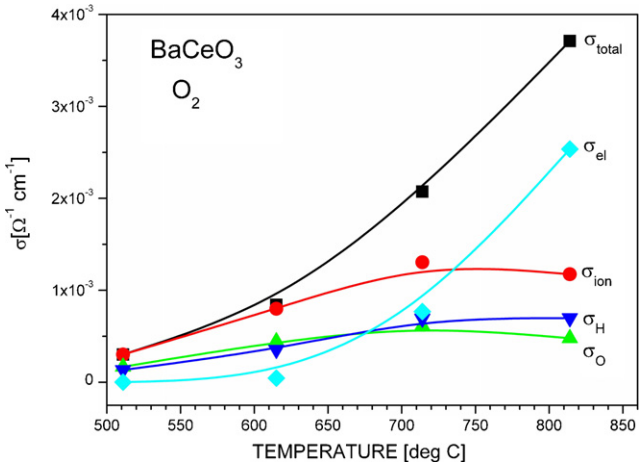

Fig. 4. Electrical conductivity versus temperature of $BaCeO_3$ in O_2 rich atmosphere (21 vol.% O_2 in N_2).

On the other hand, in oxygen rich atmosphere (Fig. 4), in particular at higher temperatures (above 750 °C), $BaCeO_3$ is predominantly an electronic semiconductor. Both oxygen and proton components assume comparable low values. Similar dependencies are observed for $BaCe_{0.95}Ti_{0.05}O_3$ at hydrogen (Fig. 5) and oxygen (Fig. 6) atmospheres.

Fig. 7 shows the comparison of temperature dependence of total electrical conductivities of several $BaCe_{1-x}Ti_xO_3$ samples in oxygen and hydrogen rich atmospheres. The lines are given for showing the general trends only. As can be seen, the introduction of titanium leads to the decrease of total electrical conductivity by ca. one order of magnitude in case of oxygen rich atmospheres and less than one order of magnitude in hydrogen rich atmospheres, almost independently of the Ti concentration in both cases.

Fig. 8 shows the transference numbers for oxygen t(O), protonic t(H) and electronic t(el) defects as a function of Ti concentration determined for different atmospheres (O_2 and H_2 rich) and selected two representative temperatures (873 K and 1073 K). As can be seen, in hydrogen rich atmospheres and

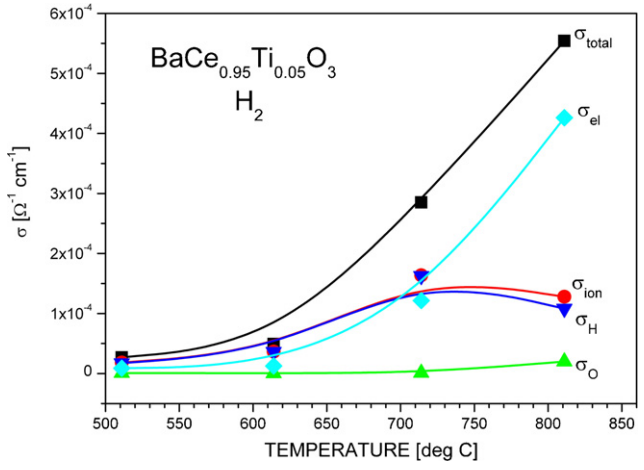

Fig. 5. Electrical conductivity versus temperature of $BaCe_{0.95}Ti_{0.05}O_3$ in H_2 rich atmosphere (7 vol.% H_2 in Ar).

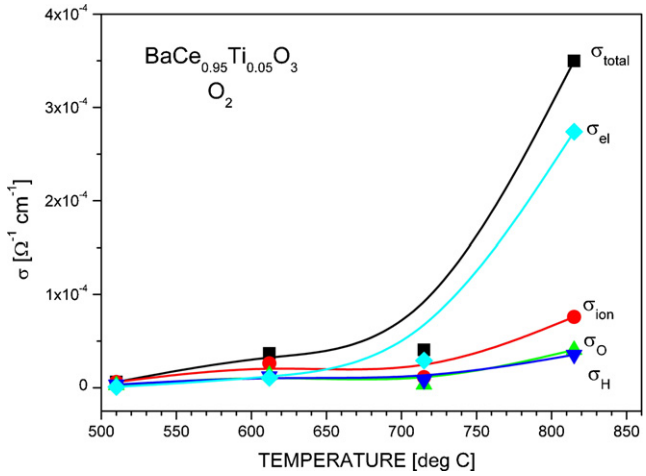

Fig. 6. Electrical conductivity versus temperature of $BaCe_{0.95}Ti_{0.05}O_3$ in O_2 rich atmosphere (21 vol.% O_2 in N_2).

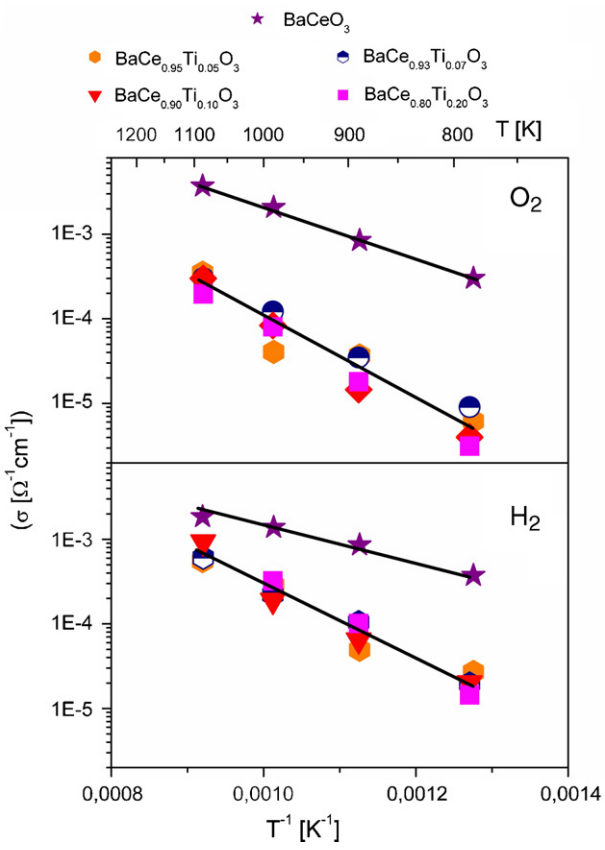

Fig. 7. The comparison of Arrhenius plots for $BaCe_{1-x}Ti_xO_3$ samples for the total conductivity in hydrogen and oxygen rich atmospheres.

lower temperatures ($T = 873$ K), the introduction of Ti leads to the gradual decrease of protonic transference number t(H) and increase of electronic transference number t(el) with increase of Ti concentration. This effect is even stronger at higher temperatures ($T = 1073$ K). In case of oxygen rich atmospheres similar dependence may be observed at lower temperatures ($T = 873$ K) while at higher temperatures the electronic conductivity is predominant almost independently of Ti concentration (t(O) = 0.7–0.9).

The presented results indicate that the optimization of transport properties of $BaCe_{1-x}Ti_xO_3$ materials is possible by careful selection of Ti concentration and working conditions (temperature, gas phase composition). Further studies and material modifications are necessary in order to increase the total electrical conductivity of the materials.

4. Conclusions

The results of XRD, SEM and DC electrical measurements presented in this paper indicate that the incorporation of titanium into the $BaCeO_3$ lattice leads to the far modification of the lattice structure, microstructure and the electrical properties. The estimated solubility limit of titanium in the $BaCeO_3$ lattice does not exceed 20% of Ti.

The positive effect of titanium incorporation is the improvement of sinterability/density of materials, comparing to the undoped materials. Moreover, Ti addition increases the electronic component of electrical conductivity, which is desirable effect in application of material in construction of membrane for hydrogen separation.

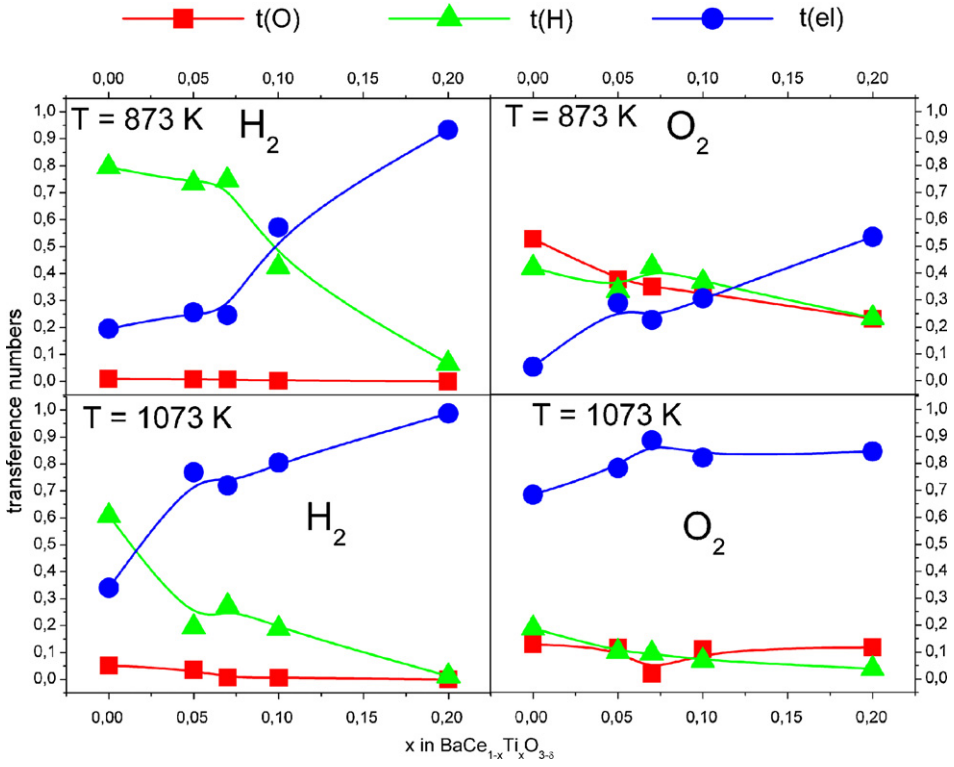

Fig. 8. The transference numbers for oxygen vacancies t(O), protonic defects t(H) and electronic carriers t(el) as a function of Ti content, (x in $BaCe_{1-x}Ti_xO_3$) for oxygen and hydrogen rich atmospheres compared for 873 K and 1073 K.

On the other hand, the introduction of Ti dopant leads to a decrease of total electrical conductivity by ca. one order of magnitude compared to the undoped material. This effect was expected analogically to the $BaCe_{1-x}Zr_xO_3$ materials. The modification of the transport properties after doping with titanium also takes place, mainly observed as a shift of electrical conductivity from ionic to electronic type. $BaCe_{1-x}Ti_xO_3$ system seems to be promising for application in hydrogen separators after further modifications leading to the increase in total electrical conductivity.

Acknowledgement

The financial support of Polish Ministry of Higher Education and Science (MEiN), Project no. K133/T02/2006 (PBZ-KBN-117/T08/03) is acknowledged.

References

[1] Hydrogen. The Fuel for the Future, DOE/GO-10095-099 DE95004024, March 1995, US Department of Energy.
[2] C.J. Winter, Int. J. Hydrogen Energy 30 (2005) 681–685.
[3] T. Bak, J. Nowotny, M. Rekas, C.C. Sorrell, Int. J. Hydrogen Energy 27 (2002) 991–1022.
[4] M. Radecka, M. Rekas, K. Zakrzewska, Trends in Inorganic Chemistry 9 (2006) 81–126.
[5] J.C. Chow, J.G. Watson, A. Herzog, S.M. Benson, G.M. Hidy, W.D. Gunter, S.J. Penkala, C.M. White, J. Air Waste Manage. Assoc. 53 (2003) 1172.
[6] C.M. White, B.R. Stazisar, E.J. Granite, J.S. Hoffman, H.W. Pennline, J. Air Waste Manage. Assoc. 53 (2003) 645.
[7] H. Iwahara, T. Esaka, H. Uchida, Y. Yamauchi, K. Ogaki, Solid State Ionics 18–19 (1986) 1003.
[8] K.D. Kreuer, Solid State Ionics 97 (1997) 1–15.
[9] C.D. Savaniu, J. Canales-Vazques, J.T.S. Irvine, J. Mater. Chem. 15 (2005) 598–604.
[10] M. Schwartz, B.S. Berland, S.K. Gade, R.W. Schaller, Abstr. Pap. Am. Chem. Soc. 225 (2003) U864.
[11] K.S. Knight, N. Bonanos, Mater. Res. Bull. 30 (1995) 347–356.
[12] A.R. Potter, R.T. Baker, Solid State Ionics 177 (2006) 1917–1924 (and Refs. [1] & [9] herein).
[13] J. Guan, S.E. Morris, U. Balachandran, M. Liu, Solid State Ionics 100 (1997) 45–52.
[14] P. Pasierb, M. Wierzbicka, S. Komornicki, M. Rekas, J. Power Sources 173 (2007) 681–687.